



## Quasi 3D polymerization in C<sub>60</sub> bilayers in a fullerene solvate



Cuiying Pei<sup>a</sup>, Meina Feng<sup>b, c, d</sup>, Zhenxing Yang<sup>d</sup>, Mingguang Yao<sup>d</sup>, Ye Yuan<sup>a</sup>, Xin Li<sup>a</sup>,  
Bingwen Hu<sup>e</sup>, Ming Shen<sup>e</sup>, Bin Chen<sup>f</sup>, Bertil Sundqvist<sup>d, g</sup>, Lin Wang<sup>a, \*</sup>

HPSTAR  
447-2017

<sup>a</sup> Center for High Pressure Science and Technology Advanced Research, 1690 Cailun Rd., Pudong District, Shanghai, 201203, China

<sup>b</sup> Institute of High Energy Physics, Chinese Academy of Sciences (CAS), Beijing, 100049, China

<sup>c</sup> Dongguan Neutron Science Center, Dongguan, Guangdong, 523803, China

<sup>d</sup> State Key Laboratory of Superhard Materials, Jilin University, Changchun, 130012, China

<sup>e</sup> Shanghai Key Laboratory of Magnetic Resonance, School of Physics and Materials Science, East China Normal University, Shanghai, 200062, China

<sup>f</sup> Hawaii Institute of Geophysics and Planetology, University of Hawaii at Manoa, Honolulu, HI, 96822, USA

<sup>g</sup> Department of Physics, Umeå University, Umeå, 90187, Sweden

### ARTICLE INFO

#### Article history:

Received 19 July 2017

Received in revised form

24 August 2017

Accepted 3 September 2017

Available online 4 September 2017

#### Keywords:

Solvate fullerene

Polymerization

High pressure

Spectroscopy

Synchrotron XRD

### ABSTRACT

The polymerization of fullerenes has been an interesting topic for almost three decades. A rich polymeric phase diagram of C<sub>60</sub> has been drawn under a variety of pressure–temperature conditions. However, only linear or perpendicular linkages of C<sub>60</sub> are found in the ordered phases. Here we used a unique bilayer structural solvate, C<sub>60</sub>·1,1,2-trichloroethane (C<sub>60</sub>·1TCAN), to generate a novel quasi-3D C<sub>60</sub> polymer under high pressure and/or high temperature. Using Raman, IR spectroscopy and X-ray diffraction, we observe that the solvent molecules play a crucial role in confining the [2 + 2] cycloaddition bonds of C<sub>60</sub>s forming in the upper and lower layers alternately. The relatively long distance between the two bilayers restricts the covalent linkage extended in a single individual bilayer. Our studies not only enrich the phase diagram of polymeric C<sub>60</sub>, but also facilitate targeted design and synthesis of unique C<sub>60</sub> polymers.

© 2017 Elsevier Ltd. All rights reserved.

### 1. Introduction

Polymeric fullerenes with different configurations are of great interest and of fundamental importance due to their superior properties and unique structure. As the most popular fullerene, C<sub>60</sub> has been extensively studied under a wide range of pressure and temperature conditions. The C<sub>60</sub> cages pack linear one-dimensional (1D, orthorhombic), 2D (tetragonal or rhombohedral) polymers and even 3D polymers in high pressure and high temperature (HPHT) conditions starting from the face centered cubic (*fcc*) lattice monomer [1–5]. The validity of these structural models are supported by the results and investigations of multi adduct regioselectivity. The [2 + 2] cycloaddition occurs preferentially at [6,6] bonds [6], and the *e* bisadduct presents a linear (or perpendicular) polymer and is favored among the eight isomers [7]. For C<sub>70</sub>, the reaction diagram contains orthorhombic, rhombohedral, tetragonal phases as well shared general features with that of C<sub>60</sub> but with significantly fewer phases [8]. As reported, a zigzag and

chain-like polymer extended along the *c* axis of C<sub>70</sub> could be obtained under high pressures and high temperatures [9]. Here, we present a quasi-3D polymerization of C<sub>60</sub> by choosing a unique fullerene solvate with a bilayer structure. This opens a new door for the design of polymeric fullerenes with different linkage configurations.

Solvated fullerenes in which C<sub>60</sub> is separated by solvent molecules are a series of crystalline materials with high stability, tunable metrics, and functionality. The intercalated solvent molecules play an important role in the construction of solvate molecules with different structures and further influence the phase transition under high pressure. For example, while the *fcc* lattice is maintained in C<sub>60</sub>·C<sub>8</sub>H<sub>8</sub> under ambient conditions due to the perfect placement of cubane in the octahedral voids [10], copolymers of C<sub>60</sub> and the decomposition product of cubane are observed when heating with high pressure [11]. Intercalation of C<sub>60</sub> with an aromatic molecule, *m*-xylene, results in C<sub>60</sub>·*m*-xylene with a hexagonal close-packed (*hcp*) structure. This exhibits no pressure-induced polymerization up to 13 GPa because of isolation from the solvent molecule [12,13]. At higher compression values, long-range ordered carbon clusters are present based on the total isolation along the three-fold axis of

\* Corresponding author.

E-mail address: [wanglin@hpstar.ac.cn](mailto:wanglin@hpstar.ac.cn) (L. Wang).

the lattice. In addition,  $C_{60}/AgNO_3$  [14,15],  $C_{60}/Ni(OEP)$  [14,15],  $C_{60}/Fe(C_5H_5)_2$  [16,17], and TDAE- $C_{60}$  (TDAE: tetrakisdimethylamino-ethylene) [18,19], etc. transformed to the one-dimensional polymeric phase when polymerized  $C_{60}S_{16}$  was in the  $b,c$ -plane [20].  $C_{60}/CS_2$  forms a 3D polymeric phase catalyst *via*  $CS_2$  under high pressure/high pressure and high temperature (HP/HPHT) conditions [21,22]. In all, the  $C_{60}$  solvate was confined by molecules regardless of particle size, aromaticity or redox reactivity. However, this has not yet been constructed as a nonlinear polymer. It is still unclear whether a properly intercalated molecule could induce the formation of a nonlinear polymer with stimuli. The answer to this question will consummate the correlation between an intercalated molecule and the fullerene cage. Furthermore, it could enrich the diversity of lattice tuning *via* an intrinsic molecule.

In this paper, the influence on the polymerization of  $C_{60}$  solvate grown from 1,1,2-trichloroethane was studied and monitored by *in-situ* Raman and Fourier transform infrared (FTIR) spectroscopy. The  $C_{60} \cdot 1TCAN$  behaves differently from other  $C_{60}$  solvates under high pressure, and a quasi-3D oligomerization in the bilayer is observed for the first time. X-ray powder diffraction (XRD) measurements were performed on a  $C_{60} \cdot 1TCAN$  to detect the lattice shrinking under high pressure. In terms of geometry structure, the intercalated solvent molecule tunes the spatial arrangement of  $C_{60}$  cages in  $C_{60} \cdot 1TCAN$ , and the steric confinement of TCAN affects the polymerization behavior of  $C_{60}$  cages under high pressure. The results of this study will help explain the diverse cross-linking fullerene derivatives and will enrich the phase diagram of polymeric  $C_{60}$ .

## 2. Results and discussion

We studied  $C_{60} \cdot 1TCAN$  due to its unique bi-layered structure [23,24] (Fig. 1). As Michaud et al. reported, the lattice metrics of the  $C_{60} \cdot 1TCAN$  solvate is orthorhombic, and the symmetry is monoclinic (space group  $P2_1/n$ ,  $a = 10.1302(5)$  Å,  $b = 31.449(2)$  Å,  $c = 10.1749(5)$  Å,  $\beta = 90.14(8)^\circ$ ). The fullerene cages stack along the  $b$  crystallographic axis. The square-like  $C_{60}$  layer has a type of AB-B'A'-AB parallel to the  $ac$  plane (Fig. 1). The orientation disordered TCAN molecule was injected between the  $C_{60}$  species and contributed to the relatively large interstitial cavities parallel to the  $b$  axis.

Group theory predicts that a  $C_{60}$  molecule have  $I_h$  symmetry as well as two  $A_g$  and eight  $H_g$  Raman-active vibrations. In situ high pressure Raman was used to study the polymerization behavior of  $C_{60} \cdot 1TCAN$  as shown in Fig. 2. For forbidden photo-polymerization, all of the *in-situ* pressure-induced Raman experiments of  $C_{60} \cdot 1TCAN$  were conducted with a 785 nm excitation laser. Two shoulder peaks at 333 and 525  $cm^{-1}$  were detected in the investigated range, and these were attributed to the C–Cl bending and  $Cl_3C$  and  $Cl_2HC$  expansion as well as contraction vibration modes of the guest solvent molecules, respectively (Supplementary Fig. 1a) [25].

Five peaks at 342, 353, 534, 567, and 579  $cm^{-1}$  could not be observed in *fcc*  $C_{60}$ . These were activated  $H_u(1)$ ,  $F_{2u}(1)$ ,  $F_{1u}(1)$ ,  $F_{1g}(1)$  and  $H_u(2)$  modes due to the symmetry reduction and the short intermolecular distance (stronger intermolecular interactions) [26]. Otherwise, this is similar to that of pristine  $C_{60}$ . Supplementary Fig. 1b shows that the Raman peaks of 1428  $cm^{-1}$ , 1470  $cm^{-1}$  and 1575  $cm^{-1}$  correspond to the pentagon shear [ $H_g(7)$ ], pentagon pinch [ $A_g(2)$ ], and hexagon shear [ $H_g(8)$ ], respectively. The other two obvious peaks at 268  $cm^{-1}$  and 493  $cm^{-1}$  are assigned to  $H_g(1)$  squashing mode and  $A_g(1)$  breathing mode, respectively. In particular, the  $A_g(2)$  is one of the most sensitive modes to the polymer structure and charge transfer. For instance, it downshifts

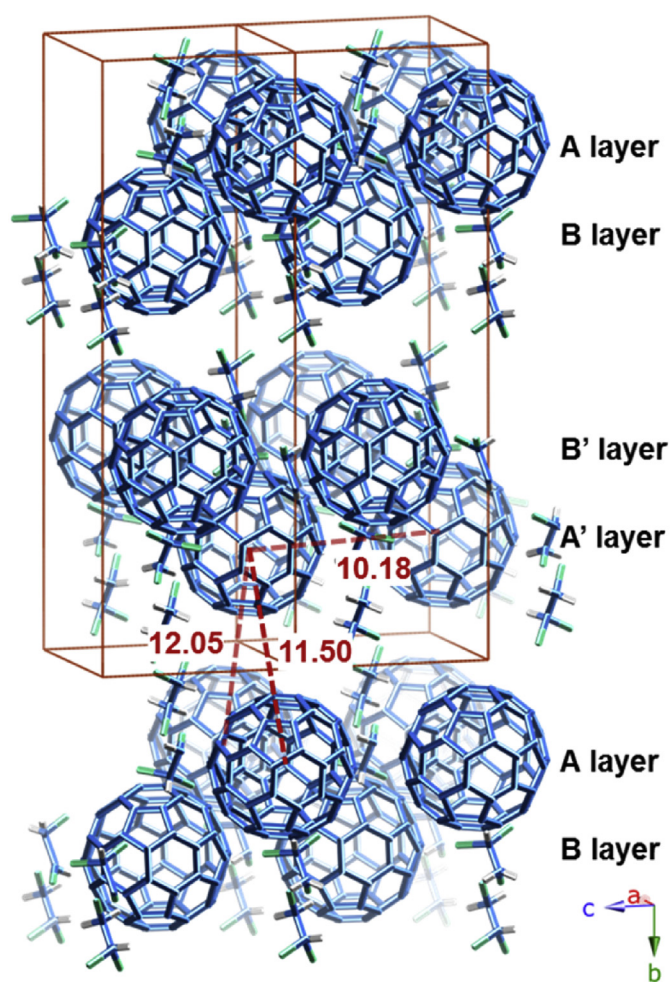


**Fig. 1.** Visualization of the refined crystal structure of the  $C_{60} \cdot 1TCAN$ . The cuboid represents the monoclinic unit cell of  $C_{60} \cdot 1TCAN$ . For clarity, only the averaged centers of mass of the  $C_{60} \cdot 1TCAN$  is shown, and some fullerenes are displayed with a transparency to better visualize the positions of the other molecules. Both the *transoid* and *gauche* TCAN conformers are present since both of them exist in the solvate molecule in ambient condition. (A colour version of this figure can be viewed online.)

from 1470  $cm^{-1}$  in the monomer to 1465  $cm^{-1}$  in the dimer—this corresponds to two  $sp^3$ -like coordinated carbon atoms per fullerene molecule [27]. Upon further polymerization, the softening is 12  $cm^{-1}$  in the linear polymeric chains [28], 20  $cm^{-1}$  in the planar tetragonal phase, and 60  $cm^{-1}$  in the 2D rhombohedral polymers [29]. The peak position of the  $A_g(2)$  mode in  $C_{60}$  and  $C_{60} \cdot 1TCAN$  are the same, and this indicates the absence of charge transfer in the solvate molecule.

As pressure increases, shifts and splitting of the icosahedral modes were observed under optimal conditions. For example, the  $H_g(1)$  and  $H_g(2)$  modes split into doublets and present shoulder peaks with a  $\sim 5$   $cm^{-1}$  shift to their parent modes at 0.7 GPa (Fig. 2). In addition, a very small but non-negligible shoulder peak was observed on the lower side of the  $A_g(2)$  mode at 0.7 GPa. Other than that, there were two new peaks at 516 and 526  $cm^{-1}$  that could be attributed to the activated  $F_{1u}(1)$  mode [29]. The peak splitting and the activation of the silent mode could be attributed to the symmetry reduction due to the lattice deformation under high pressure. In fact, traces of dimers may have already started to form here and become significant at 2.1 GPa. Two  $F_{1u}(1)$  modes at 516 and 526  $cm^{-1}$  became more obvious. A splitting of the  $H_g(1)$  mode appeared at 304  $cm^{-1}$  and a new peak ascribed to the activated

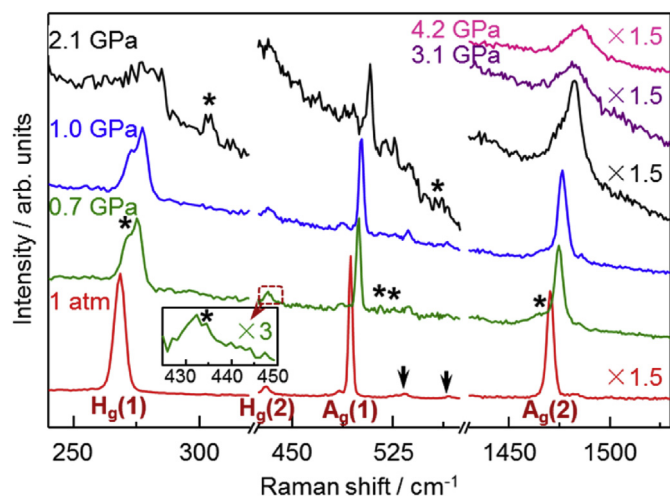


**Fig. 2.** Raman spectra of  $C_{60}\cdot 1TCAN$ . Gathered using a 785 nm excitation laser under high pressures; peaks related to the solvent molecule were marked with black arrows, new peaks were marked with stars. For clarity, the intensity of the spectra obtained at 1 atm, 2.1 GPa, 3.1 GPa and 4.2 GPa were enhanced 1.5 times. The spectrum insert was amplified 3 times in both the horizontal and vertical direction. (A colour version of this figure can be viewed online.)

$F_{1u}(2)$  mode emerged [29,30]. The most prominent includes a shoulder peak that softens to about  $5\text{ cm}^{-1}$  to low frequency of the  $A_g(2)$ . Furthermore, the full width at half maximum (FWHM) of  $A_g(2)$  mode broadens to three times than that under ambient conditions.

On the other hand, the background of Raman spectra increased from 1 atm to 2.1 GPa (Supplementary Fig. 1). A broad luminescence band is observed at 3.1 GPa and shifts to high frequency as the pressure increases. This decays over 7.1 GPa. The electronic transition in the  $C_{60}$  molecule from the lowest unoccupied electronic state (triply degenerated  $t_{1u}$  state) to the highest occupied electronic state (fivefold degenerated  $h_u$  state) is dipole forbidden [31,32]. Doping or polymerization might reduce the symmetry of the  $C_{60}$  molecule allowing previously forbidden electric-dipole transitions [33,34] to drastically enhance the photoluminescence (PL) intensity. In addition, the volume reduction and bond formation of the  $C_{60}$  cages under high pressure results in an enhanced interaction between molecules. The distortion of  $C_{60}$  cages induces a shift and broadening of the energy bands while promoting dipole-dipole transitions [35]. Furthermore, under high pressure, the exciton trapping time and the singlet to triplet conversion time should be different from that of the pristine sample [35]. The band gap also slowly decreases with increasing pressure, and the excitation becomes more efficient.

The pressure dependence of the frequency ( $d\nu/dP$ ) is determined by linearly fitting the equations. The slope of the  $A_g(2)$  frequency-pressure relationship is  $4.09\text{ cm}^{-1}\text{ GPa}^{-1}$  at a low pressure range. It slightly decreases to  $3.15\text{ cm}^{-1}\text{ GPa}^{-1}$ . The pressure-dependence of the peak positions of the main Raman modes are shown in Supplementary Fig. 2. Although all peaks besides  $A_g(2)$  are difficult to detect over 3 GPa, peak splitting is seen near 0.7 GPa. The inflection point is  $\sim 2.1$  GPa and is obviously present in these modes. This might be because the lattice symmetry decreases with increasing pressure leading to significant dimer formation. These dimers are precursors to larger oligomers which are found over  $\sim 2.1$  GPa.

To further study the structural changes of  $C_{60}\cdot 1TCAN$  at the inflection points seen in Supplementary Fig. 2, the Raman spectra of the samples decompressed from 3.1 GPa, 4.0 GPa, 7.6 GPa, 8.3 GPa,

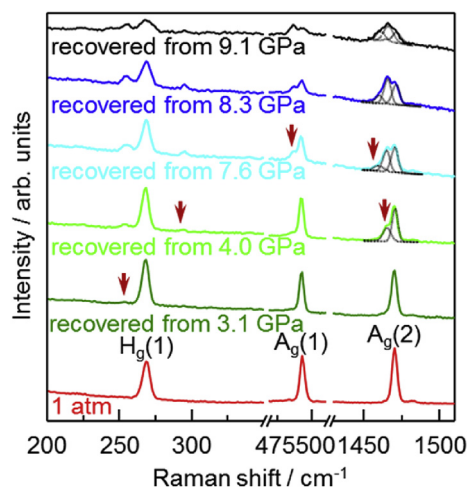


**Fig. 3.** Raman spectra of pristine  $C_{60}\cdot 1TCAN$  and recovered samples to 1 atm from different pressures. The new peaks are marked with red arrows. (A colour version of this figure can be viewed online.)

and 9.1 GPa were collected using a 785 nm laser as shown in Fig. 3. All of the vibrational peaks corresponding to the cage structure remain after decompression. This suggests that the  $C_{60}$  cage was preserved. However, the recovered samples show more and broader bands than the pristine sample indicating a decrease in symmetry. On another hand, the disordered dimer/polymer orientation and the degree of polymerization can also attribute to the broadening, as shown in pristine  $C_{60}$  [30].

For instance, the  $H_g(1)$  mode presents a low-frequency peak at  $252\text{ cm}^{-1}$  recovered from 3.1 GPa. There is another weak peak at  $295\text{ cm}^{-1}$  when decompressed from 4.0 GPa. This is an obvious feature of  $C_{60}$  dimerization [29]. Furthermore, the  $I_{255}/I_{268}$  (the intensity of the peak at  $255\text{ cm}^{-1}$  over that of the peak at  $268\text{ cm}^{-1}$ ) increased with increasing pressure. This is a feature of high molecule weight  $C_{60}$  polymerization [29]. At the same time, the shoulder of the  $A_g(1)$  mode appeared when the sample was decompressed from 7.6 GPa. As reported, the  $A_g(1)$  mode softens  $6\text{ cm}^{-1}$  for the dimer and  $8\text{ cm}^{-1}$  in the orthorhombic polymer [29]. This new shoulder confirms that the mixture phase contains the monomer and  $C_{60}$  with one or two cycloaddition bonds.

As the pressure further increases, the low-frequency constitute is enriched compared with the high-frequency one. The  $A_g(2)$  mode softens at a low frequency as the number of covalent bonds per  $C_{60}$  increases [27–29]. No significant changes were found when the sample decompressed from 3.1 GPa. It split into two peaks with the new peak near  $1465\text{ cm}^{-1}$  when recovered from 4.0 GPa. The  $1465\text{ cm}^{-1}$  peak is attributed to the  $C_{60}$  dimer [29], and this demonstrates strong dimerization above 3 GPa. As the pressure increased, a new Raman active mode is expected for the  $C_{60}$  polymer with two cycloaddition bonds near  $1460\text{ cm}^{-1}$ . This was observed in the sample recovered from 7.6 GPa and coincided with the results obtained from the  $H_g(1)$  and  $A_g(1)$  modes. The peak area ratios of  $1470\text{ cm}^{-1}$ ,  $1465\text{ cm}^{-1}$  and  $1460\text{ cm}^{-1}$  follow a regular trend with degree of polymerization. The proportion of the peak at  $1470\text{ cm}^{-1}$  decreased when the sample decompressed from 3.1 GPa to 9.1 GPa. At the same time, the area of the peak at  $1460\text{ cm}^{-1}$  increased as the pressure increased from 7.6 GPa to 9.1 GPa. This showed that the  $C_{60}$  dimer combines into larger units and was confirmed by the appearance of Raman signals from molecules with two cycloaddition bonds. As expected, the peak area at  $1460\text{ cm}^{-1}$  increased when accompanied by a deepening of the degree of polymerization. Hence, pressure induces new types of



intermolecular interactions and corresponding vibrations that possibly explain the resolved Raman bands that are absent in the pristine sample. In conclusion, there is significant dimerization at pressures over 3.1 GPa. These dimers start to polymerize over 7.6 GPa. This concurs with the pressure dependence data.

The formation of intermolecular bonds of  $C_{60}$  is a thermally activated process, and the polymerization reaction is very slow at room temperature. Thus  $C_{60}$ -1TCAN treated under HPHT could potentially synthesize the polymer phase. The Raman spectra of the recovered  $C_{60}$ -1TCAN after treatment at 1.2 GPa and 573 K is shown in Fig. 4. In contrast to  $C_{60}$  that contains ~75% disordered “chains” and approximately 20% dimers in the same condition [36], polymerized and unpolymerized  $C_{60}$  coexist in the treated  $C_{60}$ -1TCAN. The peak areas showed that a small proportion of  $C_{60}$  transformed to a dimer-rich phase and barely contains polymer with two cycloaddition bonds on  $C_{60}$ . Versus the cold compression of  $C_{60}$ -1TCAN, the polymerization degree is larger under high temperature, but still smaller than that of  $C_{60}$  under HPHT conditions.

To enhance the degree of polymerization, higher pressures (3.0 GPa and 4.6 GPa) were used in the HPHT treatment. A doublet splitting of the  $H_g(1)$  mode was seen as a shoulder in the low-frequency range combined with an activated  $G_g(1)$  mode at  $\sim 473\text{ cm}^{-1}$  when the sample was recovered from 4.6 GPa to 573 K. In fact, these results were seen on the sample recovered from 3.0 GPa/573 K although it is not as obvious as the sample treated by 4.6 GPa/573 K. Moreover, the  $A_g(2)$  contains two component near 1464 and  $1458\text{ cm}^{-1}$  with a few at  $1469\text{ cm}^{-1}$ . In addition, the  $I_{1458}/I_{1464}$  (the intensity of the peak at  $1458\text{ cm}^{-1}$  over that of the peak at  $1464\text{ cm}^{-1}$ ) increased with compression. It contains almost all of the  $C_{60}$  monomer that participated in the reaction. The proportion of polymer increased as the treatment pressure increased. More than 50% of the molecules have two cycloaddition bonds and others have a single bond as shown in the disordered dimers. These results suggest that high temperature facilitates polymerization, but formation of pure polymer from  $C_{60}$ -1TCAN is harder than that of  $C_{60}$  even under HPHT conditions.

Based on these considerations, the polymerization procedure becomes gradually clear. The short nearest distance between the  $C_{60}$  cages in the  $C_{60}$ -1TCAN makes the dimerization occur more easily. Bond formation causes local strain, although the positions of

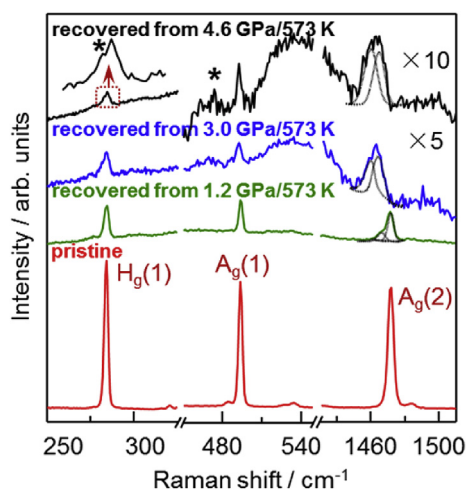


**Fig. 4.** Raman spectra of pristine  $C_{60}$ -1TCAN and samples treated by high pressure and high temperature. Samples are treated at 1.2 GPa, 573 K, 20000 s (olive), 3.0 GPa, 573 K, 20000 s (blue) and 4.6 GPa, 573 K, 20000 s (black). For clarity, all the peak intensities of sample treated under 3.0 GPa, 573 K, 20000 s are multiply 5 and sample treated under 4.6 GPa, 573 K, 20000 s are multiply 10. (A colour version of this figure can be viewed online.)

neighboring atomic will slightly change to offset the void. The increasing distance between the unreacted monomers is insufficient for further dimerization. As a result, the dimerization of  $C_{60}$ -1TCAN occurs at a lower pressure than that of  $C_{60}$  and the degree of dimerization is lower than that of  $C_{60}$  treated under the same condition. On the other hand,  $C_{60}$  dimers meet more steric hindrance when they are rearranged to the optimal position and orientation compared to  $C_{60}$  monomer. Furthermore, the disordered dimer-monomer mixture makes positional and orientational matching more challenging.

For these reasons, further cycloaddition to get a polymer with high molecule weight (HMW) is unlikely. High temperature can promote cage rotation and is conducive to HMW polymers. However, faster intermolecular cycloaddition causes low completeness of dimerization. Consequently, cycloaddition is enhanced under high temperature, but no pure polymer with a HMW has yet been obtained. The same phenomenon has been observed in other doped  $C_{60}$  such as  $C_{60}$ /ferrocene [16]. The incomplete polymerization reasons were classified into three parts: layered packing arrangement, insufficient reduction of the volume at the polymerization pressure used and competing  $C_{60}$  orientational ordering [14].

FTIR is another useful method to probe structural transformation under high pressure. It is well known that an isolated  $C_{60}$  molecule has four IR-active vibrational modes at 527, 576, 1183, and  $1429\text{ cm}^{-1}$ . These are attributed to  $F_{1u}(1)$ ,  $F_{1u}(2)$ ,  $F_{1u}(3)$  and  $F_{1u}(4)$  symmetries, respectively [37]. For  $C_{60}$ -1TCAN, the vibrational modes are at the same position because of the weak van der Waals intermolecular interactions. Besides, seven vibration modes belonging to the TCAN molecule are observed in the FTIR spectrum (Fig. 5).

Upon pressure-induced polymerization, the intermolecular bonds provide a strong new interaction mechanism to break the  $I_h$  symmetry of the isolated  $C_{60}$ . As a result, numerous new Raman and IR modes are observed. These are attributed to both the formed covalent intermolecular bond and the intramolecular bonds because of the reduced symmetry. The position and shape of the  $F_{1u}(4)$  mode is sensitive to both the charged state and the covalent numbers per cage [38]. In the IR spectrum of the dimer, three modes with odd symmetry at 711, 754 and  $799\text{ cm}^{-1}$  were attributed to  $F_{2u}(2)$ ,  $G_u(3)$  and  $F_{2u}(3)$ , respectively. These are present when the samples are compressed to 1.7 GPa. The splitting of  $F_{1u}(3)$

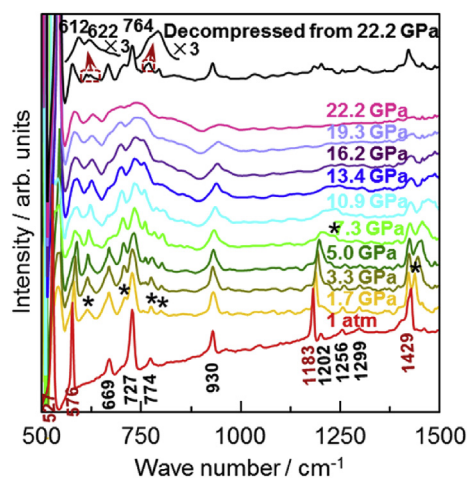


**Fig. 5.** FTIR spectra of  $C_{60}$ -1TCAN with pressure ranging from 1 atm to 22.2 GPa and recovered to 1 atm from 22.2 GPa. Peaks related to the solvent molecule were marked in black, while attributed to the  $C_{60}$  cage were in red. New peaks were marked with stars. For clarity, part of the range was amplified 3 times in both the horizontal and vertical direction. (A colour version of this figure can be viewed online.)

in the polymer is more pronounced when the bands appear at 1207 and 1234  $\text{cm}^{-1}$  under high pressure (7.3 GPa). Although several reports have summarized 1426 ( $F_{1u}(4)$ ) and 1464  $\text{cm}^{-1}$  ( $A_g(2)$ ) as the two vibration modes for the  $C_{60}$  dimer and 1426 ( $F_{1u}(4)$ ), 1446  $\text{cm}^{-1}$  ( $F_{1u}(4)$ ) for  $C_{60}$  orthorhombic polymer, it is easy to distinguish the two dimer peaks but hard to determine the weak and broad peaks in the spectrum of the orthorhombic polymer. Thus, we conclude that the sample dimerized near 1.7 GPa and polymerized from 7.9 GPa to 10.9 GPa. This nicely correlates to the Raman measurements.

The resonance at 612  $\text{cm}^{-1}$  is absent under ambient condition but becomes very prominent under high pressure. This is because the  $H_u(2)$  mode has features that are characteristic of the pressure-polymerized  $C_{60}$  indicating modification of the cage. The  $C_{60}$  dimer shows a peak at 613  $\text{cm}^{-1}$ , which shifts to 614  $\text{cm}^{-1}$  at 1.7 GPa. The doublet at 612 and 622  $\text{cm}^{-1}$  of  $C_{60}\cdot 1\text{TTCAN}$  decompressed from 22.2 GPa indicates that the product is different from the  $C_{60}$  dimer and orthorhombic polymer. This is in contrast to the  $C_{60}$  dimer and the orthorhombic  $C_{60}$  polymer with the  $H_u(2)$  mode at 613  $\text{cm}^{-1}$  and 612  $\text{cm}^{-1}$  [29], respectively. Of note, a shoulder peak at 764  $\text{cm}^{-1}$  could not be observed in orthorhombic  $C_{60}$  polymers, but this can be seen in the two-dimensional tetragonal one [39]. Perhaps the 612  $\text{cm}^{-1}$  peak may still be from dimers, however some novel spectroscopy features do not from a straight, linear chain system. Hence the high-pressure polymeric phase is quite different from known  $C_{60}$  polymers.

Polymeric  $C_{60}\cdot 1\text{TTCAN}$  produced by large volume press under high pressure and high temperature is characterized using  $^{13}\text{C}$  magic angle spinning nuclear magnetic resonance (MAS NMR) measurements at room temperature. As shown in Supplementary Fig. 3, several resonances between 160 and 65 ppm have been observed besides the partial carbon fragment at around 30 ppm. Two isotropic lines at positions 70 and 50 ppm are attributed to the solvent while typical  $\text{sp}^3$  carbon evidence for the formation of covalent bonds between cages is overlapped at 70 ppm. Broad line around 146 ppm corresponds to a continue distribution of C–C distances due to a partial disorder. Deconvolution result exhibits a refinement structure. The clear peak splitting at 146 ppm is a further manifestation for inequivalence of the two carbon atoms bridging neighboring molecules in the polymeric phase [9,40].

It is important to discuss geometry structure to explain the stability of  $C_{60}\cdot 1\text{TTCAN}$  and the degree of polymerization. Starting

from the disordered  $C_{60}$  dimers, a low-pressure 1D orthorhombic phase characterized by different orientations of the chains around their axes has been found [41]. Parallel straight chains along one of the six  $\langle 110 \rangle$  directions were present at high-pressure (above 2–3 GPa). However, it is impossible for this to occur on  $C_{60}\cdot 1\text{TTCAN}$ . The TCAN molecule parted four near-neighbored cages in one layer and [2 + 2] cycloaddition bonds alternately connect the  $C_{60}$  cages in the upper and lower layers. Thus, polymerization is confined to single individual bilayers in the  $ac$  plane with no bonds between bilayers.

Bisadditions at [6,6]-junctions of  $C_{60}$  enable eight regioisomers [7]. The *e* and *trans*-3 bisadducts were generally formed preferentially by a (2 + 2) cycloaddition reaction among the eight isomers. However, in  $C_{60}\cdot 1\text{TTCAN}$ , as shown in Fig. 6, cage II, III, IV, and V are the four fullerenes nearest to cage I. If the first cycloaddition occurred between cage I of the  $A'$  layer and cage II of the  $B'$  layer (shown as the first adduct position with blue double bond in Fig. 6a), then cage III and V are near the location of the *e* addition site and cage IV is near the location of *trans*-3. This demonstrates that polymers with more than three  $C_{60}$  cages prefer to form a V-shaped or N-shaped polymer (Fig. 6b and Supplementary Fig. 4). Of note, the cage position and orientation are expected to change to get a stable product.

The distance between the center of mass position of two near-neighbored  $C_{60}$  in the *fcc* bulk  $C_{60}$  is 10.1 Å [10], and the minimum in  $C_{60}\cdot 1\text{TTCAN}$  is 8.8 Å—a much smaller value (Fig. 1). As a result, the overlap of  $\pi$  orbitals in  $C_{60}\cdot 1\text{TTCAN}$  is larger than that of  $C_{60}$ , which is beneficial to dimerization. The center-to-center  $C_{60}$ – $C_{60}$  distances decrease as pressure increases. Generally, it is 9.1 Å in  $C_{60}$  [2 + 2] cycloaddition polymers and about 9.4 Å when a single C–C bond links two cages [5,42,43]. For confined  $C_{60}$ , the nearest-neighbor cage distance could approach a value of 8.45 Å near 10 GPa [44]. The much shorter  $C_{60}$ – $C_{60}$  distance in  $C_{60}\cdot 1\text{TTCAN}$  causes easier dimerization accompanied by a low degree of polymerized structure. In addition, the nearest two cages in  $C_{60}\cdot 1\text{TTCAN}$  penetrate AB bilayers or  $A'B'$  bilayers. The minimum distance between the two cages in the same layer is 10.13 Å along the *an* axis. The nearest cage distance along the *c* axis is 10.18 Å and along the *b* axis is as long as 11.50 Å.

These results indicate that polymerization of  $C_{60}\cdot 1\text{TTCAN}$  is confined to single individual bilayers in the  $ac$  plane with no bonds between the bilayers under high pressure. Similar to the  $C_{60}$  cages

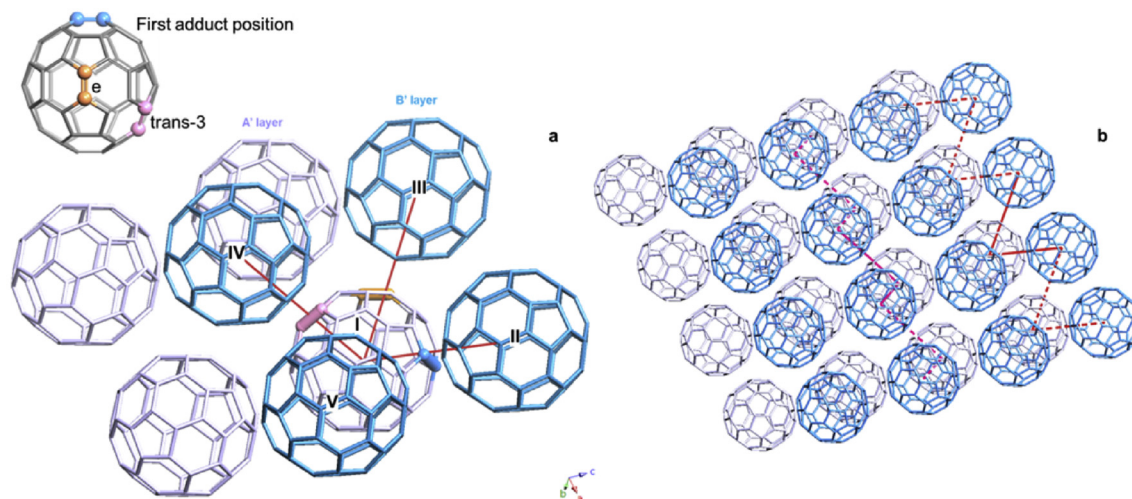


**Fig. 6.** Regioselective bisadduct of fullerene. (a) Visualization of the  $B'A'$  layer of the refined  $C_{60}\cdot 1\text{TTCAN}$  crystal structure and the possible  $C_{60}$  bisadduct regioisomer configurations of cage I. (b) red and pink lines exhibit two possible orientations of the polymerization. (A colour version of this figure can be viewed online.)

in a bilayer, these structures are sutured with covalent bonds. After dimerization, rearrangement and reorientation of the cages can create an available steric configuration for further polymerization. This is more difficult to realize on a dimer than on a monomer, though the lattice volume reduction after dimerization allows other molecules to take up positions that are favorable for further dimer formation. In addition, tuning the disordered dimers to match the binding site in a nonlinear chain is much harder. Consequently, quasi-3D oligomerization in a 2D bilayer structure is obtained here, which coincides well with the experiment results.

The structure changes under high pressure were confirmed by XRD, as shown in [Supplementary Fig. 5](#). The position and orientation disorder of the C<sub>60</sub> moieties leads to broad diffraction profiles. Although it is hard to refine the Bragg peaks, the main peaks in the pattern could be indexed. It should be noted that an identifiable new peak ( $2\theta = 2.78^\circ$ ) appears at 3.7 GPa and becomes obvious with pressure increasing. The appearance of this peak is an indication of structure change caused by the polymerization. However, the high pressure phase can not be solved reliably with the limited number of the peaks.

We studied the variation in d spacing of the (040) lattice plane as the pressure increased from 0.3 GPa to 8.2 GPa ([Supplementary Fig. 6](#)) and found that it shifted from 8.135 Å to 7.571 Å as the pressure increased. This demonstrates that the change in lattice parameter b is around 0.141 Å. Accordingly, the distance between near-neighbor bilayers decreases with increasing pressure, but the gap over 11 Å confirms that it is impossible to form a covalent bond along the b axis under high pressure. Hence, the XRD data confirm our geometry structure analysis and the vibration experimental results again.

The effect of TCAN on the structure and properties of C<sub>60</sub>·1TCAN under high pressure could be summarized as below. First, TCAN with a medium particle size between CS<sub>2</sub> and aromatic intercalated molecules expands the cubic lattice to a monoclinic structure with a relative isolated bilayer configuration in C<sub>60</sub> cages along the b axis. Second, C<sub>60</sub> is relatively insoluble in TCAN, which implies a weaker interaction between injected molecules and the carbon cage. As a result, TCAN is not wrapped tightly around the cage, with room for the polymerization and confines the cross-linking in certain orientations. Third, the stability of TCAN ensures polymerization under HP/HPHT condition. Based on these considerations, the principle behind quasi-3D oligomerization in a bilayer structure is clearly explained.

### 3. Conclusion

In this work, we successfully synthesized a quasi-3D oligomer of C<sub>60</sub> by compressing C<sub>60</sub>·1TCAN—a solvate with unique bilayer C<sub>60</sub> structure. The *in situ* Raman and infrared measurements under high pressures suggested that the high dimer fraction presented at about 2.1 GPa. A polymer with C<sub>60</sub> cages linked in the upper and lower layers started to form above 7.9 GPa. The data show that about 50% molecules have a single cycloaddition bond, and approximately 50% have two bonds. No single molecules (without any intermolecular bonds) are seen, and the sample must be fully oligomerized. In addition, FTIR shows signs of dimers but also lines belonging to a hitherto not observed polymeric phase, which different from the known chains or known 2D phases. The structure of C<sub>60</sub>·1TCAN and its polymeric phases were determined by XRD showing that the C<sub>60</sub>s bridged into the polymer that extend along the single individual bilayers in the ac plane of the parent structure under high pressure. Our results demonstrate the crucial role of the TCAN solvent molecule in initial lattice structure design and polymerization confinement under HP/HPHT.

### Acknowledgment

This work is supported by the fund of National Science Associated Funding (NSAF, Grant No. U1530402), Science Challenging Program (Grant No. JCKY2016212A501), Postdoctoral Science Foundation (2015M572499) and U.S. National Science Foundation (EAR-1555388).

### Appendix A. Supplementary data

Supplementary data related to this article can be found at <https://doi.org/10.1016/j.carbon.2017.09.010>.

### References

- [1] A.M. Rao, P. Zhou, K.-A. Wang, G.T. Hager, J.M. Holden, Y. Wang, et al., Photoinduced polymerization of solid C<sub>60</sub> films, *Science* 259 (1993) 955–957.
- [2] M. Núñez-Regueiro, L. Marques, J.L. Hodeau, O. Béthoux, M. Perroux, Polymerized fullerite structures, *Phys. Rev. Lett.* 74 (1995) 278–281.
- [3] Y. Iwasa, T. Arima, R.M. Fleming, T. Siegrist, O. Zhou, R.C. Haddon, et al., New phases of C<sub>60</sub> synthesized at high pressure, *Science* 264 (1994) 1570–1572.
- [4] R.S. Ruoff, A.L. Ruoff, Is C<sub>60</sub> stiffer than diamond? *Nature* 350 (1991) 663–664.
- [5] M. Álvarez-Murga, J.L. Hodeau, Structural phase transitions of C<sub>60</sub> under high-pressure and high-temperature, *Carbon* 82 (2015) 381–407.
- [6] J.P. Martínez, F. Langa, F.M. Bickelhaupt, S. Osuna, M. Solà, (4+2) and (2+2) cycloadditions of benzyne to C<sub>60</sub> and Zig-Zag single walled carbon nanotubes: the effect of the curvature, *J. Phys. Chem. C* 120 (2016) 1716–1726.
- [7] Y. Nakamura, N. Takano, T. Nishimura, E. Yashima, M. Sato, T. Kudo, et al., First isolation and characterization of eight regioisomers for [60]fullerene-benzyne bisadducts, *Org. Lett.* 3 (2001) 1193–1196.
- [8] B. Sundqvist, Polymeric fullerene phases formed under pressure, *Struct. Bond.* 109 (2004) 85–126.
- [9] A.V. Soldatov, G. Roth, A. Dzyabchenko, D. Johnels, S. Lebedkin, C. Meingast, et al., Topochemical polymerization of C<sub>70</sub> controlled by monomer crystal packing, *Science* 293 (2001) 680–683.
- [10] S. Pekker, É. Kováts, G. Oslányi, G. Bényel, G. Klupp, G. Bortel, et al., Rotor-stator molecular crystals of fullerenes with cubane, *Nat. Lett.* 4 (2005) 764–767.
- [11] A. Iwasiewicz-Wabnig, B. Sundqvist, É. Kováts, I. Jalsovszky, S. Pekker, Polymerization of the rotor-stator compound C<sub>60</sub>-cubane under pressure, *Phys. Rev. B* 75 (2007), 024114.
- [12] L. Wang, B. Liu, D. Liu, M. Yao, Y. Hou, S. Yu, B. Sundqvist, et al., Synthesis of thin, rectangular C<sub>60</sub> nanorods using m-xylene as a shape controller, *Adv. Mater.* 18 (2006) 1883–1888.
- [13] L. Wang, B. Liu, H. Li, W. Yang, Y. Ding, S. Sinogeikin, et al., Long-range ordered carbon clusters: a crystalline material with amorphous building blocks, *Science* 337 (2012) 825–828.
- [14] W. Cui, B. Sundqvist, S. Sun, M. Yao, B. Liu, High pressure and high temperature induced polymerization of doped C<sub>60</sub> materials, *Carbon* 109 (2016) 269–275.
- [15] W. Cui, S. Sun, B. Sundqvist, S. Wang, B. Liu, Pressure induced metastable polymerization in doped C<sub>60</sub> materials, *Carbon* 115 (2017) 740–745.
- [16] W. Cui, M. Yao, D. Liu, Q. Li, R. Liu, B. Zou, et al., Reversible polymerization in doped fullerenes under pressure: the case of C<sub>60</sub>(Fe(C<sub>5</sub>H<sub>5</sub>)<sub>2</sub>)<sub>2</sub>, *J. Phys. Chem. B* 116 (2012) 2643–2650.
- [17] K. Kato, H. Murata, H. Gonnokami, M. Tachibana, Polymerization in ferrocene-doped C<sub>60</sub> nanosheets under high pressure and light irradiation, *Carbon* 107 (2016) 622–628.
- [18] K. Mizoguchi, M. Takei, H. Sakamoto, T. Kawamoto, M. Tokumoto, A. Omerzu, et al., Uniaxial strain study in purely organic ferromagnet  $\alpha$ -TDAE-C<sub>60</sub>-Mechanism and structure, *Polyhedron* 24 (2005) 2173–2175.
- [19] K. Mizoguchi, M. Machino, H. Sakamoto, T. Kawamoto, M. Tokumoto, A. Omerzu, et al., Pressure effect in TDAE-C<sub>60</sub> ferromagnet: mechanism and polymerization, *Phys. Rev. B* 63 (2001), 140417(R).
- [20] A.V. Talyzin, L.S. Dubrovinsky, U. Jansson, High pressure Raman study of C<sub>60</sub>S<sub>16</sub>, *Solid State Comm.* 123 (2002) 93–96.
- [21] M. Du, M. Zhao, M. Yao, P. Ge, S. Chen, X. Yang, et al., High pressure infrared spectroscopy study on C<sub>60</sub>·CS<sub>2</sub> solvates, *Chem. Phys. Lett.* 669 (2016) 49–53.
- [22] M. Popov, V. Mordkovich, S. Perfilov, A. Kirichenko, B. Kulnitskiy, I. Perezhogin, et al., Synthesis of ultrahard fullerite with a catalytic 3D polymerization reaction of C<sub>60</sub>, *Carbon* 76 (2014) 250–256.
- [23] F. Michaud, M. Barrio, D.O. López, J.L. Tamarit, V. Agafonov, S. Toscani, et al., Solid-state studies on a C<sub>60</sub> solvate grown from 1,1,2-trichloroethane, *Chem. Mater.* 12 (2000) 3595–3602.
- [24] E. Mitsari, M. Romanini, N. Qureshi, J.L. Tamarit, M. Barrio, R. Macovez, C<sub>60</sub> solvate with (1,1,2)-trichloroethane: dynamic statistical disorder and mixed conformation, *J. Phys. Chem. C* 120 (2016) 12831–12839.
- [25] Gordon F. Hull Jr., Comparison of the Raman spectra of 1,1,1- and 1,1,2-trichloroethane, *J. Chem. Phys.* 3 (1935) 534–535.
- [26] L. Wang, B. Liu, S. Yu, M. Yao, D. Liu, Y. Hou, et al., Highly enhanced

- luminescence from single-crystalline  $C_{60}$ -1m-xylene nanorods, *Chem. Mater.* 18 (2006) 4190–4194.
- [27] T. Wågberg, P. Jacobsson, B. Sundqvist, Comparative Raman study of photopolymerized and pressure-polymerized  $C_{60}$  films, *Phys. Rev. B* 60 (1999) 4535–4538.
- [28] V.M. Senyavin, V.A. Davydov, L.S. Kashevarova, A.V. Rakhmanina, V. Agafonov, H. Allouchi, et al., Spectroscopic properties of individual pressure-polymerized phases of  $C_{60}$ , *Chem. Phys. Lett.* 313 (1999) 421–425.
- [29] V.A. Davydov, L.S. Kashevarova, A.V. Rakhmanina, V.M. Senyavin, R. Céolin, H. Swarc, et al., Spectroscopic study of pressure-polymerized phases of  $C_{60}$ , *Phys. Rev. B* 61 (2000) 11936–11945.
- [30] R. Moret, P. Launois, T. Wågberg, B. Sundqvist, V. Agafonov, V.A. Davydov, et al., Single-crystal structural study of the pressure-temperature-induced dimerization of  $C_{60}$ , *Eur. Phys. J. B* 37 (2004) 25–37.
- [31] R.C. Haddon, L.E. Brus, K. Raghavachari, Electronic structure and bonding in icosahedral  $C_{60}$ , *Chem. Phys. Lett.* 125 (1986) 459–464.
- [32] F. Negri, G. Orlandi, F. Zerbetto, Quantum-chemical investigation of Franck-Condon and Jahn-Teller activity in the electronic spectra of Buckminsterfullerene, *Chem. Phys. Lett.* 144 (1988) 31–37.
- [33] Y. Wang, J.M. Holden, A.M. Rao, P.C. Eklund, U.D. Venkateswaran, D. Eastwood, et al., Optical absorption and photoluminescence in pristine and photopolymerized  $C_{60}$  solid films, *Phys. Rev. B* 51 (1995) 4547–4556.
- [34] Y. Zhao, Y. Fang, Fluorescence of  $C_{60}$  and its interaction with pyridine, *J. Phys. Chem. B* 108 (2004) 13586–13588.
- [35] I.O. Bashkin, A.N. Izotov, A.P. Moravsky, V.D. Negrii, R.K. Nikolaev, Yu A. Ossipyan, et al., Photoluminescence of solid  $C_{60}$  polymerized under high pressure, *Chem. Phys. Lett.* 272 (1997) 32–37.
- [36] B. Sundqvist, Mapping intermolecular bonding in  $C_{60}$ , *Sci. Rep.* 4 (2014), 06171.
- [37] M.S. Dresselhaus, G. Dresselhaus, P.C. Eklund, *Science of Fullerenes and Carbon Nanotubes: the Properties and Applications*, Laszlo Nemes, Academic Press, Inc., 1996.
- [38] M. Krause, D. Deutsch, P. Janda, L. Kavan, L. Dunsch, Electrochemical nanostructuring of fullerene films-spectroscopic evidence for  $C_{60}$  polymer formation and hydrogenation, *Phys. Chem. Chem. Phys.* 7 (2005) 3179–3184.
- [39] A.M. Rao, P.C. Eklund, U.D. Venkateswaran, J. Tucker, M.A. Duncan, G.M. Bendele, et al., Properties of  $C_{60}$  polymerized under high pressure and temperature, *Appl. Phys. A* 64 (1997) 231–239.
- [40] F. Rachdi, C. Goze, L. Hajji, M. Núñez-Regueiro, L. Marques, J.-L. Hodeau, et al., High resolution  $^{13}C$  NMR studies of one- and two-dimensional polymerized  $C_{60}$  under high pressure, *J. Phys. Chem. Solids* 58 (1997) 1645–1647.
- [41] R. Moret, Structures, phase transitions and orientational properties of the  $C_{60}$  monomer and polymers, *Acta Cryst. A* 61 (2005) 62–76.
- [42] V.A. Davydov, L.S. Kashevarova, A.V. Rakhmanina, A.V. Dzyabchenko, V.N. Agafonov, P. Dubois, et al., Identification of the polymerized orthorhombic phase of  $C_{60}$  fullerene, *JETP Lett.* 66 (1997) 120–125.
- [43] S. Margadonna, K. Prassides, Recent advances in fullerene superconductivity, *J. Solid State Chem.* 168 (2002) 639–652.
- [44] S. Kawasaki, T. Hara, T. Yokomae, F. Okino, H. Touhara, H. Kataura, et al., Pressure-polymerization of  $C_{60}$  molecules in a carbon nanotube, *Chem. Phys. Lett.* 418 (2006) 260–263.